LETTERS
https://doi.org/10.1038/s41566-018-0317-y

nature photonics

Electronically programmable photonic molecule

Mian Zhang[1,7], Cheng Wang[1,2,7], Yaowen Hu[1,3], Amirhassan Shams-Ansari[1,4], Tianhao Ren[1,5], Shanhui Fan[6] and Marko Lončar[1*]

Physical systems with discrete energy levels are ubiquitous in nature and acre fundamental building blocks of quantum technology. Realizing controllable artificial atom- and molecule-like systems for light would enable coherent and dynamic control of the frequency, amplitude and phase of photons[1–5]. In this work, we demonstrate a 'photonic molecule' with two distinct energy levels using coupled lithium niobate microring resonators and control it by external microwave excitation. We show that the frequency and phase of light can be precisely controlled by programmed microwave signals, using concepts of canonical two-level systems including Autler–Townes splitting, Stark shift, Rabi oscillation and Ramsey interference. Through such coherent control, we show on-demand optical storage and retrieval by reconfiguring the photonic molecule into a bright–dark mode pair. These results of dynamic control of light in a programmable and scalable electro-optic system open doors to applications in microwave signal processing[6], quantum photonic gates in the frequency domain[7] and exploring concepts in optical computing[8] and topological physics[3,9].

Photonic analogues of condensed-matter systems have resulted in discoveries such as photonic crystals[5], parity–time symmetric systems[2] and topological photonic systems[3,9], and have led to technologies including quantum ground-state cooling of nanomechanical systems[10], new classes of sensors[11,12] and one-way lasers[4]. A photonic analogue of a two-level system could allow full control over the energy and phase of photons by using the concept of two-level systems control in atomic or molecular systems, where the state of the electron can be controlled and functionalized by external electromagnetic fields. Such a photonic system would enable the investigation of complex physical phenomena[2–4,7] and unique functionalities, including on-demand photon storage and retrieval, coherent optical frequency shift and optical quantum information processing at room temperature[7,13,14]. Although it is straightforward to realize a photonic device with discrete energy levels, for example by using modes of an optical resonator, controlling such a system dynamically (that is, inducing transitions between the levels) is challenging as it requires mixing of optical frequencies through strong nonlinear processes. As a result, coherent coupling between discrete photon energy modes has only been studied using all-optical methods[14–17] and has limited design parameter space, configurability and scalability.

Electro-optic methods[6,18–23] are ideally suited for the dynamic control of photonic two-level systems, since they have fast response, can be programmed and allow for large-scale integration. To realize coherent electro-optic control of a photonic two-level system, the photon lifetime of each energy state needs to be much longer than the time required to drive the system from one state to the other. On the one hand, large optical systems with optical amplifiers[24] can emulate a classical two-level system, but the quantum coherence of the optical photons is destroyed in the process. On the other hand, conventional integrated photonic platforms have not been able to meet the requirements of long photon lifetime and fast modulation simultaneously. For example, fast phase modulators[7,25] can generate new optical frequencies, but they do not support distinct and long-lived optical modes. On-chip resonators with ultra-high quality factors (Q) have traditionally been realized in passive materials, such as silicon dioxide (SiO_2)[26,27] and silicon nitride (Si_3N_4)[28,29], which can only be controlled electrically using slow thermal effects. Electrically active photonic platforms[18–22] based on silicon[18], III–V materials[15,20], plasmonic[19], graphene[22] and polymers[21] allow for fast electro-optic modulation at gigahertz frequencies, but suffer from much shorter photon lifetimes than passive platforms. To circumvent this problem, out-of-plane picosecond optical pulses have been used to induce a broadband electro-optic tuning in silicon via ultrafast free carriers[16,30]. Purely electrical tuning is still highly desirable as narrowband microwave signals could offer much better controllability, minimal added noise and scalability.

In this work, we overcome the existing performance trade-off and realize a programmable photonic two-level system that can be dynamically controlled by gigahertz microwave signals (Fig. 1a). Specifically, we create a microwave-addressable photonic molecule using a pair of integrated lithium niobate microring resonators, 80 μm in radius, patterned close to each other. The low optical loss[31] and efficient co-integration of optical waveguides and microwave electrodes[32,33] allow us to simultaneously achieve large electrical bandwidth (>30 GHz), strong modulation efficiency (0.5 GHz V^{-1}) and long photon lifetime (~2 ns).

The photonic molecule supports a pair of well-defined optical energy levels, which are evident from the optical transmission measured using a tunable telecom-wavelength laser (Fig. 1c; see Supplementary Information for full spectrum). The two optical energy levels are formed by the evanescent coupling of light from one resonator to another through a 500-nm gap. When the optical coupling strength μ exceeds the optical loss rate γ of each cavity, the coupling leads to a normal mode splitting resulting in a frequency doublet consisting of a lower-frequency symmetric (S) and a higher-frequency antisymmetric (AS) optical mode (Fig. 1a and c). The S (AS) mode spatially spans both optical cavities, with the light in the two cavities being in-phase (out-of-phase). The two new eigenmodes, separated in frequency by $2\mu = 2\pi \times 7$ GHz, are the two energy levels of the photonic molecule. In our case, the two optical modes have cavity linewidths of $\gamma = 2\pi \times 96$ MHz, corresponding

[1]John A. Paulson School of Engineering and Applied Sciences, Harvard University, Cambridge, MA, USA. [2]Department of Electronic Engineering, City University of Hong Kong, Kowloon, Hong Kong, China. [3]Department of Physics, Tsinghua University, Beijing, China. [4]Department of Electrical Engineering and Computer Science, Howard University, Washington, DC, USA. [5]University of Electronic Science and Technology of China, Chengdu, China. [6]Ginzton Laboratory and Department of Electrical Engineering, Stanford University, Palo Alto, CA, USA. [7]These authors contributed equally: Mian Zhang, Cheng Wang. *e-mail: loncar@seas.harvard.edu

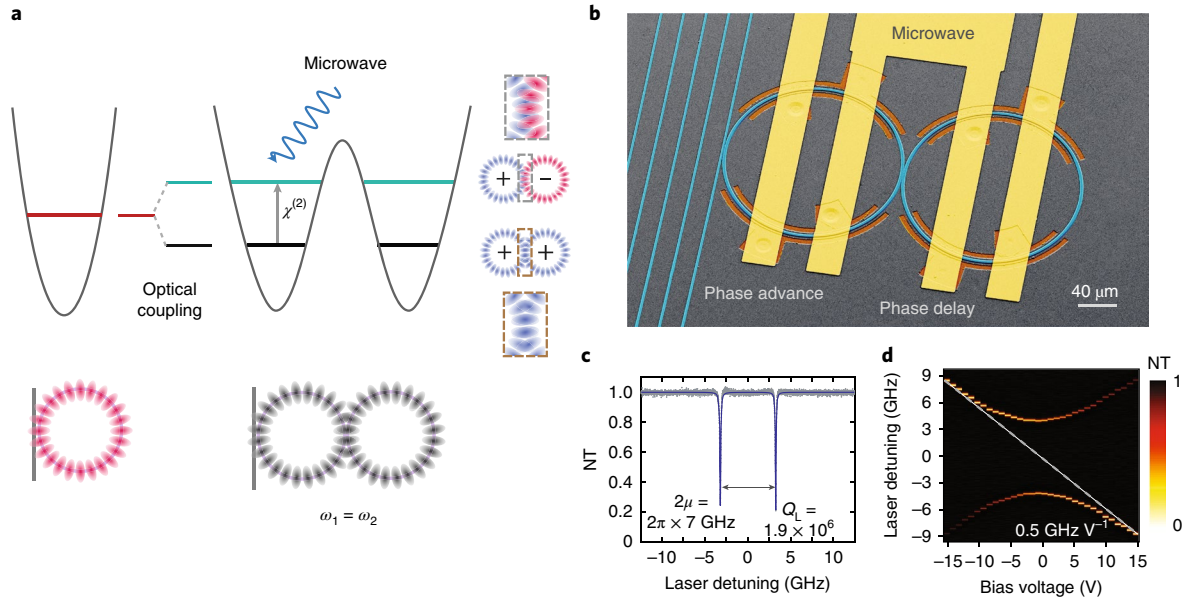

Fig. 1 | Microwave-controlled photonic molecule. a, The photonic molecule is realized by a pair of identical coupled optical microring resonators (resonant frequency $\omega_1 = \omega_2$). The system has two distinct energy levels—a symmetric and an antisymmetric optical mode (indicated here by blue/blue shading for the symmetric and red/blue for the antisymmetric mode) that are spatially out of phase by π. The microwave field can interact coherently with the two-level system through the strong Pockels effect ($\chi^{(2)}$) of lithium niobate. **b**, False-coloured scanning electron microscope image of the coupled microring resonators. **c**, Measured transmission spectrum of the photonic two-level system. The two optical modes are separated by $2\mu = 2\pi \times 7$ GHz with linewidths of $\gamma = 2\pi \times 96$ MHz corresponding to a loaded optical quality factor of 1.9×10^6. **d**, The resulting transmission spectra from an applied d.c. field show an anticrossing curve due to the finite optical coupling between the two rings, which is analogous to the d.c. Stark effect in a canonical two-level system. NT, normalized transmission.

to a loaded quality factor of $Q_L = 1.9 \times 10^6$ (intrinsic quality factor $Q_i = 2.5 \times 10^6$), thus forming a well-resolved two-level system (Fig. 1c).

We induce photonic transitions in the two-level system using high-frequency electro-optic phase modulation of the two modes. The phase modulation is realized through the Pockels effect ($\chi^{(2)}$) for lithium niobate, in which the optical refractive index can be changed by an applied electric field, with a response time on the femtosecond scale. To enable strong overlap between microwave and optical fields without significantly increasing the optical loss, we place gold microelectrodes 2.5 μm away from the edge of the rings that form the photonic molecule (Fig. 1b). The microwave circuit layout is designed to induce a phase delay in one ring and a phase advance in the other ring, therefore introducing coupling between the spatially orthogonal S and AS modes (Fig. 1a and Supplementary Information).

We explore the analogy between an atomic two-level system and the photonic two-level system, and use it to demonstrate the control of the photonic molecule. In our system, the electro-optic effect plays the equivalent role to an electric dipole moment in an atomic two-level system, while in both systems external electromagnetic fields are used to couple and address their energy levels. In the presence of an external direct-current (d.c.) electric field, the resonance frequencies of the two rings are pulled in opposite directions. This added frequency detuning reduces the optical coupling between the two resonators and results in the characteristic avoided crossing curve in coupled resonator systems (Fig. 1d). The resonator frequency detuning is accomplished by applying a d.c. bias voltage in the range of ±15 V to the microwave electrodes. This control is analogous to the d.c. Stark effect used in atomic systems. The extracted tuning/modulation efficiency $g = 2\pi \times 0.5$ GHz V^{-1} is an order of magnitude larger than previously demonstrated in bulk electro-optic resonator systems[34,35], and is due to the efficient overlap between microwave and optical fields enabled by our system (see Methods).

Next, we use a continuous-wave coherent microwave field to control our photonic two-level system. This situation is similar to an atomic two-level system under a strong coherent excitation, with the important difference that in our case the number of photons that could populate each of the two levels is not limited to one. When the microwave frequency matches the energy difference of the two levels, an effective coupling between the two initially decoupled S and AS modes is introduced, leading to a second-order mode splitting in the coupled ring resonators. The exact splitting frequency (Ω) can be precisely controlled up to several gigahertz by controlling the amplitude of the microwave signals. This microwave-induced photonic mode splitting is a dissipative coupling between the optical modes in analogy to the Autler–Townes splitting (Rabi splitting) in electronic systems (Fig. 2a,b) resonantly excited with continuous-wave light. When the microwave frequency is detuned far from the transition frequency, the microwave-induced photonic coupling becomes weaker, and an effective dispersive effect in the level splitting dominates, similar to the a.c. Stark shift in atomic systems (Fig. 2c). Importantly, this effect can be used to control the effective coupling strength between the energy levels of the photonic molecule, which are otherwise determined by geometric factors.

We demonstrate that the photonic molecule can be used for unitary transformation of light in the frequency domain by controlling the dispersive and dissipative coupling between the two optical modes. In the context of two-level systems, such control over the amplitude and phase is described by Rabi oscillation and Ramsey interference (see Supplementary Information). The dynamics of the photonic two-level system can be directly visualized through the time evolution of the output photons. We apply a microwave field at the mode-splitting frequency to drive dissipative optical coupling (that is, Rabi oscillations) between the two levels of our photonic molecule (Fig. 3), similar to Autler–Townes splitting measurements (Fig. 2b). The observed Rabi oscillation corresponds to a rotation along the real axis of the energy Bloch sphere (Fig. 3c, inset) and

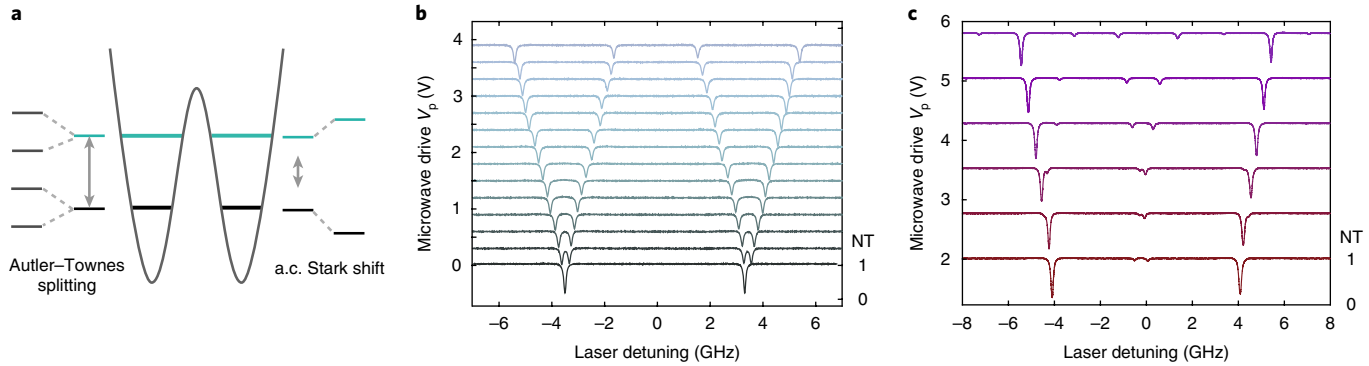

Fig. 2 | Microwave-dressed photonic states. a, When the applied microwave frequency is tuned to match the mode separation, dissipative coupling leads the two photonic levels to split into four levels. This effect is analogous to Autler–Townes splitting. When the microwave is detuned far from the photonic mode splitting, the photonic energy levels experience a dispersive effect, leading to a shift in the photonic levels. This effect is analogous to a.c. Stark shifts. **b**, Measured Autler–Townes splitting in the photonic molecule, where the splitting can be accurately controlled by the amplitude of the applied microwave signal. **c**, Measured photonic a.c. Stark shifts for a microwave signal at 4.5 GHz.

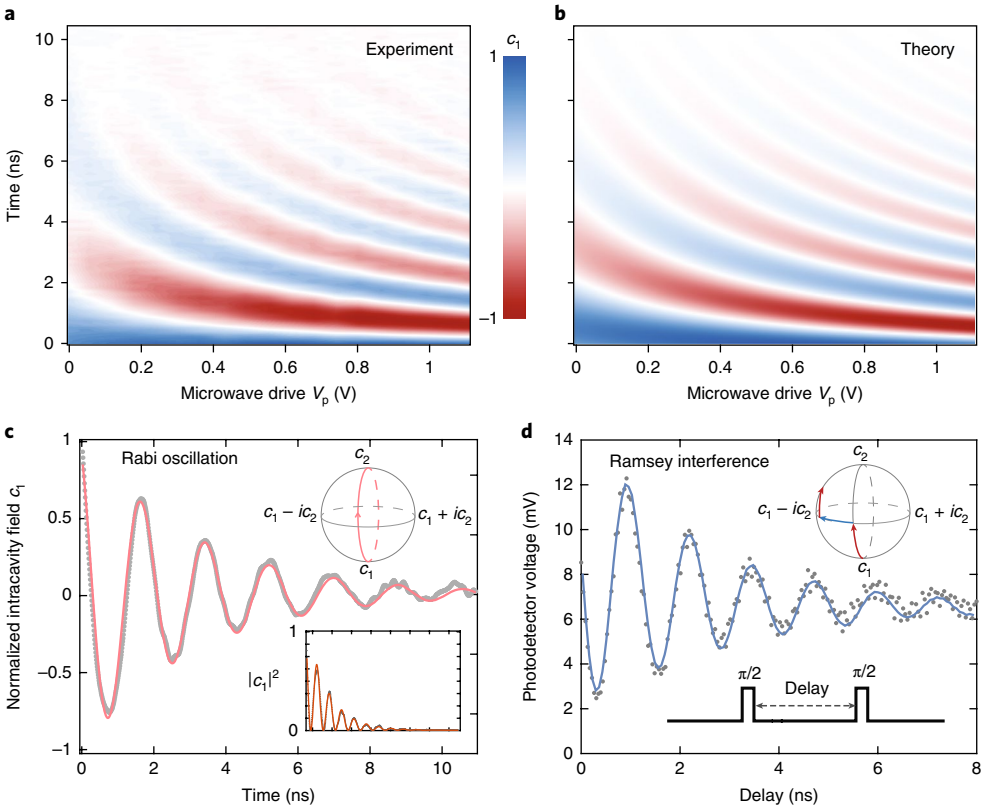

Fig. 3 | Coherent spectral dynamics in the photonic molecule. a,**b**, Measured (**a**) and theoretically predicted (**b**) coherent oscillation between the two optical modes (Rabi oscillation) for various microwave strengths applied to the photonic two-level system. As the microwave field is turned on at $t = 0$, light oscillates between the two energy levels c_1 and c_2 leading to the observed signals. **c**, Rabi oscillation at 1.1 GHz observed for microwave $V_p = 1.1$ V. This corresponds to rotation along the real axis of the Bloch sphere. Inset shows the corresponding optical intensity in mode c_1. **d**, Oscillatory signals measured on a photodetector when δ-detuned microwave $\pi/2$ pulses are applied (photonic analogy of Ramsey interference). The first $\pi/2$ pulse prepares the light in a superposition of the two optical modes with a precession frequency determined by δ. The second $\pi/2$ pulse with a delay τ maps the light with oscillating projections onto c_1 resulting in the measured interference fringes. The solid curve shows the calculated signal (see Supplementary Information).

indicates that light tunnels back and forth between the two optical modes at two different optical frequencies. In other words, using the language of nonlinear optics, the applied microwave signal drives a sequence of resonance-enhanced sum- and difference-frequency generation processes that result in the energy of photons being changed several times (more than 10 in Fig. 3c) before photons are eventually dissipated because of the cavity photon loss (cavity lifetime ~1.6 ns). To study the Rabi oscillation, we initialize the system by coupling a continuous-wave laser into the S mode and measure the real-time optical transmission as the microwave drive is turned on (see Methods and Supplementary Information). We achieve a large range of Rabi frequencies at low applied voltages (Fig. 3a),

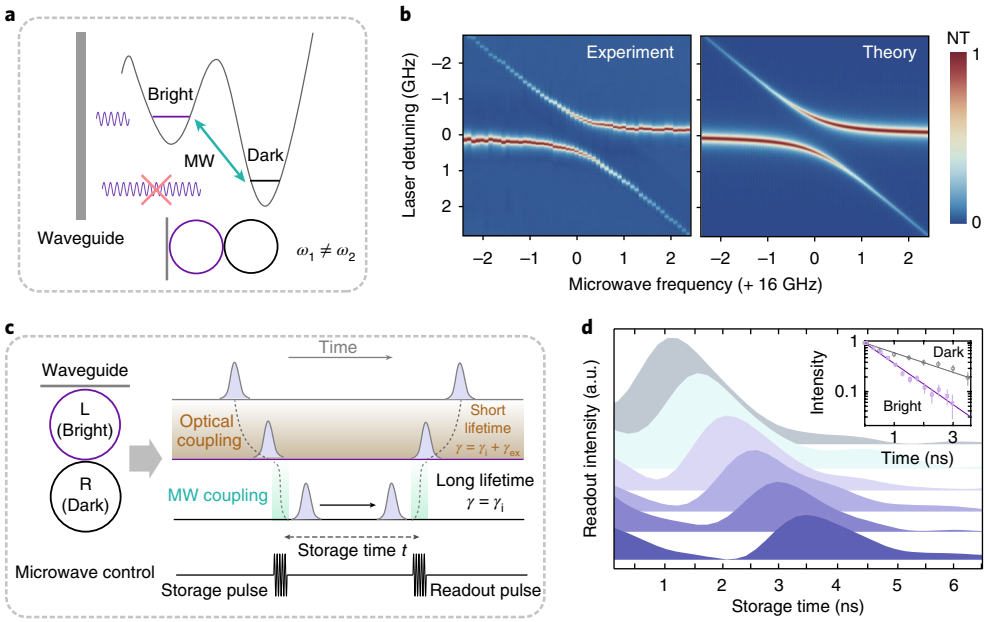

Fig. 4 | On-demand storage and retrieval of light using a photonic dark mode. a, The photonic molecule is programmed so that $\omega_1 \neq \omega_2$, resulting in localized bright and dark modes. As a result, the bright mode can be accessed from the optical waveguide, while the dark mode cannot (forbidden by geometry). **b**, A microwave field applied to the system can induce an effective coupling between the bright and dark modes, indicated by the avoided crossing in the optical transmission spectrum. **c**, Light can be deterministically stored and retrieved using the bright–dark mode pair and microwave control. A microwave π pulse can be applied to transfer light from the bright to the dark mode. As the microwave is turned off, light is restricted from any external waveguide coupling. After a certain desired storage time, a second microwave π pulse retrieves the light from the dark to the bright mode. γ, γ_i and γ_{ex} are the lifetimes of the bright optical mode, intrinsic damping and waveguide coupling rate, respectively. **d**, The retrieved light from the dark mode measured at different time delays, shown by the traces from top to bottom with a 0.5 ns delay increment. Inset: the extracted intensity of the retrieved light shows nearly twice the lifetime of the critically coupled bright mode. The error bars show the uncertainty in the optical intensity readout. MW, microwave; NT, normalized transmission; a.u., arbitrary units.

which is in excellent agreement with theoretical predictions (Fig. 3b and Supplementary Information). In particular, for a peak drive voltage of $V_p = 1.1$ V, we observe coherent Rabi oscillation with a frequency of 1.1 GHz, ~16% of the initial mode splitting. Even stronger driving regimes, where the Rabi frequencies are close to or even exceed the level splitting, could be accessible in our system, enabling the exploration of extreme conditions in which the rotating-wave approximation completely breaks down[36].

To show the control over the relative phase of the two photonic levels in our system (that is, rotation along the imaginary axis), we measure photonic Ramsey interference by driving optical transition with detuned microwave pulses at 7.8 GHz that induces a dispersive element in the optical coupling. After initializing the system in the S mode, we apply a microwave π/2 pulse to transform the optical field into a superposition of the two states. As the microwave is turned off for a time period of τ, the superposition state precesses along the equator of the Bloch sphere at a rate determined by the microwave detuning δ. After a further microwave π/2 pulse, the photons are rotated to different energy states, determined by the delay τ, and measured using a photodetector. The result is the 'Ramsey interference' shown in Fig. 3d. As the optical lifetime of the two-level system (~1.6 ns) is much shorter than the coherence time of the laser (of the order of microseconds), the phase coherence time of the two energy levels obtained in this measurement is dominated by cavity dissipation, in good agreement with that obtained from the Rabi oscillation.

We make use of the ability to perform unitary transformations in the frequency domain to achieve on-demand photon storage and retrieval—a critical task for optical signal processing. Although a static resonator can be used to slow down the propagation of a photon, such slow-down is fundamentally limited by the frequency bandwidth of the resonator (that is, the delay–bandwidth product) and cannot be controlled on demand. In contrast, the use of a dynamically modulated resonator system can overcome the constraint imposed by the delay–bandwidth limit, enabling new functionalities such as optical buffering[37]. To enable controllable write and read of light into a resonator from an external waveguide, the optical coupling strength needs to be altered faster than the photon lifetime in the cavity. To achieve this, we apply a large d.c. bias voltage (15 V) to reconfigure the double-ring system into a pair of bright and dark modes. In this limit, one of the modes is mainly localized in the first ring (purple in Fig. 4a), and thus is still accessible to the input optical waveguide and is optically bright, whereas the other mode is mainly localized in the second ring (grey in Fig. 4a) and thus is decoupled from the input optical waveguide by geometry and becomes optically dark (see Supplementary Information for details). Notably, optical access to the dark optical mode can be granted by applying a microwave signal with the frequency matched to the difference between the two optical modes (Fig. 4a). The microwave modulation results in an effective coupling between the bright and the dark mode, which we directly observe from the avoided crossing in the spectrum of the bright optical mode (Fig. 4b). In our experiment, the waveguide coupling is designed to be critically coupled to a single resonator, maximizing the transmission extinction ratio. We excite the critically coupled bright mode from the optical waveguide, and then apply a microwave π pulse to switch light from the bright to the dark mode (Fig. 4c). Once the microwave signal is turned off, the photons are trapped in the dark mode and become decoupled from the waveguide, leaving cavity intrinsic dissipation as the only photon loss mechanism. After a desired

storage time, we apply another microwave π pulse to deterministically retrieve the photons from the dark mode back into the bright mode and then into the optical waveguide (Fig. 4c). Tracking the intensity of the retrieved light, we extract a dark mode lifetime of 2 ns, which is about twice the lifetime of the critically coupled bright mode, as expected (Fig. 4d). Using an over-coupled bright optical mode, while further improving the quality factor of the integrated lithium niobate resonators towards its material limit ($>10^9$), could result in a tunable storage time of hundreds of nanoseconds (see Supplementary Information).

Our demonstration of the coherent and dynamic control of a two-level photonic molecule with microwave fields and on-demand photon storage and retrieval opens a path to a new form of control over photons. These results represent the initial step towards integrated electro-optic coherent manipulation of photonic states and energies, and could have immediate applications in signal processing and quantum photonics. With microwave control and the possible integration of on-chip photonic components including filters, routers and modulators, a new generation of photonic-electronic systems with advanced functionalities can be put in practice. Considering the vast design parameter space of couple resonators, dynamically controlled two-level and multi-level photonic systems could lead to a new class of photonic technologies including topological photonics[9], advanced photonic computation concepts[8,38] and on-chip frequency-based optical quantum systems[7,13].

Online content

Any methods, additional references, Nature Research reporting summaries, source data, statements of data availability and associated accession codes are available at https://doi.org/10.1038/s41566-018-0317-y.

Received: 4 July 2018; Accepted: 9 November 2018;
Published online: 14 December 2018

References

1. Morandotti, R., Peschel, U., Aitchison, J. S., Eisenberg, H. S. & Silberberg, Y. Experimental observation of linear and nonlinear optical Bloch oscillations. *Phys. Rev. Lett.* **83**, 4756–4759 (1999).
2. Regensburger, A. et al. Parity–time synthetic photonic lattices. *Nature* **488**, 167–171 (2012).
3. Lu, L., Joannopoulos, J. D. & Soljačić, M. Topological photonics. *Nat. Photon.* **8**, 821–829 (2014).
4. Bandres, M. A. et al. Topological insulator laser: experiments. *Science* **359**, eaar4005 (2018).
5. Joannopoulos, J. D., Villeneuve, P. R. & Fan, S. Putting a new twist on light. *Nature* **386**, 143–149 (1997).
6. Capmany, J. & Novak, D. Microwave photonics combines two worlds. *Nat. Photon.* **1**, 319–330 (2007).
7. Kues, M. et al. On-chip generation of high-dimensional entangled quantum states and their coherent control. *Nature* **546**, 622–626 (2017).
8. McMahon, P. L. et al. A fully programmable 100-spin coherent Ising machine with all-to-all connections. *Science* **354**, 614–617 (2016).
9. Lin, Q., Xiao, M., Yuan, L. & Fan, S. Photonic Weyl point in a two-dimensional resonator lattice with a synthetic frequency dimension. *Nat. Commun.* **7**, 13731 (2016).
10. Chan, J. et al. Laser cooling of a nanomechanical oscillator into its quantum ground state. *Nature* **478**, 89–92 (2011).
11. Hodaei, H. et al. Enhanced sensitivity at higher-order exceptional points. *Nature* **548**, 187–191 (2017).
12. Chen, W., Özdemir, Ş. K., Zhao, G., Wiersig, J. & Yang, L. Exceptional points enhance sensing in an optical microcavity. *Nature* **548**, 192–196 (2017).
13. O'Brien, J. L. Optical quantum computing. *Science* **318**, 1567–1570 (2007).
14. Ramelow, S. et al. Strong nonlinear coupling due to induced photon interaction on a Si_3N_4 chip. Preprint at https://arxiv.org/abs/1802.10072 (2018).
15. Guo, X., Zou, C.-L., Jung, H. & Tang, H. X. On-chip strong coupling and efficient frequency conversion between telecom and visible optical modes. *Phys. Rev. Lett.* **117**, 123902 (2016).
16. Sato, Y. et al. Strong coupling between distant photonic nanocavities and its dynamic control. *Nat. Photon.* **6**, 56–61 (2012).
17. Clemmen, S., Farsi, A., Ramelow, S. & Gaeta, A. L. Ramsey interference with single photons. *Phys. Rev. Lett.* **117**, 223601 (2016).
18. Xu, Q., Schmidt, B., Pradhan, S. & Lipson, M. Micrometre-scale silicon electro-optic modulator. *Nature* **435**, 325–327 (2005).
19. Ayata, M. et al. High-speed plasmonic modulator in a single metal layer. *Science* **358**, 630–632 (2017).
20. Shambat, G. et al. Ultra-low power fiber-coupled gallium arsenide photonic crystal cavity electro-optic modulator. *Opt. Express* **19**, 7530–7536 (2011).
21. Enami, Y. et al. Hybrid polymer/sol-gel waveguide modulators with exceptionally large electro-optic coefficients. *Nat. Photon.* **1**, 180–185 (2007).
22. Liu, M. et al. A graphene-based broadband optical modulator. *Nature* **474**, 64–67 (2011).
23. Wade, M. T., Zeng, X. & Popović, M. A. Wavelength conversion in modulated coupled-resonator systems and their design via an equivalent linear filter representation. *Opt. Lett.* **40**, 107–110 (2015).
24. Spreeuw, R. J. C., van Druten, N. J., Beijersbergen, M. W., Eliel, E. R. & Woerdman, J. P. Classical realization of a strongly driven two-level system. *Phys. Rev. Lett.* **65**, 2642–2645 (1990).
25. Karpiński, M., Jachura, M., Wright, L. J. & Smith, B. J. Bandwidth manipulation of quantum light by an electro-optic time lens. *Nat. Photon.* **11**, 53–57 (2017).
26. Armani, D. K., Kippenberg, T. J., Spillane, S. M. & Vahala, K. J. Ultra-high-*Q* toroid microcavity on a chip. *Nature* **421**, 925–928 (2003).
27. Lee, H. et al. Chemically etched ultrahigh-Q wedge-resonator on a silicon chip. *Nat. Photon.* **6**, 369–373 (2012).
28. Ji, X. et al. Ultra-low-loss on-chip resonators with sub-milliwatt parametric oscillation threshold. *Optica* **4**, 619–624 (2017).
29. Bauters, J. F. et al. Ultra-low-loss high-aspect-ratio Si_3N_4 waveguides. *Opt. Express* **19**, 3163–3174 (2011).
30. Konoike, R. et al. On-demand transfer of trapped photons on a chip. *Sci. Adv.* **2**, e1501690 (2016).
31. Zhang, M., Wang, C., Cheng, R., Shams-Ansari, A. & Lončar, M. Monolithic ultra-high-*Q* lithium niobate microring resonator. *Optica* **4**, 1536–1537 (2017).
32. Guarino, A., Poberaj, G., Rezzonico, D., Degl'Innocenti, R. & Gunter, P. Electro-optically tunable microring resonators in lithium niobate. *Nat Photon.* **1**, 407–410 (2007).
33. Witmer, J. D. et al. High-*Q* photonic resonators and electro-optic coupling using silicon-on-lithium-niobate. *Sci. Rep.* **7**, 46313 (2017).
34. Rueda, A. et al. Efficient microwave to optical photon conversion: an electro-optical realization. *Optica* **3**, 597–604 (2016).
35. Savchenkov, A. A. et al. Tunable optical single-sideband modulator with complete sideband suppression. *Opt. Lett.* **34**, 1300–1302 (2009).
36. Casanova, J., Romero, G., Lizuain, I., García-Ripoll, J. J. & Solano, E. Deep strong coupling regime of the Jaynes–Cummings model. *Phys. Rev. Lett.* **105**, 263603 (2010).
37. Yanik, M. F. & Fan, S. Stopping light all optically. *Phys. Rev. Lett.* **92**, 083901 (2004).
38. Shen, Y. et al. Deep learning with coherent nanophotonic circuits. *Nat. Photon.* **11**, 441–446 (2017).

Acknowledgements

This work was supported in part by National Science Foundation grants (ECCS1609549, DMR-1231319), Office of Naval Research MURI grant N00014-15-1-2761 and the Army Research Laboratory Center for Distributed Quantum Information W911NF1520067, Center for Integrated Quantum Materials (CIQM) and Harvard Office of Technology Development Accelerator. Device fabrication was performed at the Center for Nanoscale Systems at Harvard University.

Author contributions

M.Z., C.W., S.F. and M.L. conceived the experiment. M.Z., C.W. and A.S.-A. fabricated the devices. M.Z. and Y.H. performed numerical simulations. M.Z., C.W. and T.R. carried out the experiments. M.Z. wrote the manuscript with contribution from all authors. M.L. supervised the project.

Competing interests

M.Z., C.W. and M.L. are involved in developing lithium niobate technologies at HyperLight Corporation.

Additional information

Supplementary information is available for this paper at https://doi.org/10.1038/s41566-018-0317-y.

Reprints and permissions information is available at www.nature.com/reprints.

Correspondence and requests for materials should be addressed to M.L.

Publisher's note: Springer Nature remains neutral with regard to jurisdictional claims in published maps and institutional affiliations.

nature photonics

SUPPLEMENTARY INFORMATION

https://doi.org/10.1038/s41566-018-0317-y

In the format provided by the authors and unedited.

Electronically programmable photonic molecule

Mian Zhang[1,7], Cheng Wang[1,2,7], Yaowen Hu[1,3], Amirhassan Shams-Ansari[1,4], Tianhao Ren[1,5], Shanhui Fan[6] and Marko Lončar[1*]

[1]John A. Paulson School of Engineering and Applied Sciences, Harvard University, Cambridge, MA, USA. [2]Department of Electronic Engineering, City University of Hong Kong, Kowloon, Hong Kong, China. [3]Department of Physics, Tsinghua University, Beijing, China. [4]Department of Electrical Engineering and Computer Science, Howard University, Washington, DC, USA. [5]University of Electronic Science and Technology of China, Chengdu, China. [6]Ginzton Laboratory and Department of Electrical Engineering, Stanford University, Palo Alto, CA, USA. [7]These authors contributed equally: Mian Zhang, Cheng Wang. *e-mail: loncar@seas.harvard.edu

Supplementary Material: Programmable Photonic Molecule

Mian Zhang,[1] Cheng Wang,[1] Yaowen Hu,[1,2] Amirhassan Shams-Ansari,[1,3] Tianhao Ren,[1,4] Shanhui Fan,[5] and Marko Loncar[1]

[1] *John A. Paulson School of Engineering and Applied Sciences, Harvard University, Cambridge, Massachusetts 02138, USA*
[2] *Department of Physics, Tsinghua University, Beijing, 100084, China*
[3] *Department of Electrical Engineering and Computer Science, Howard University, Washington DC 20059, USA.*
[4] *University of Electronic Science and Technology of China, Chengdu, 611731, China*
[5] *Ginzton Laboratory and Department of Electrical Engineering, Stanford University, Palo Alto, California 94305, USA*

(Dated: October 17, 2018)

APPENDIX S-1: DEVICE AND EXPERIMENTAL SETUP DETAILS

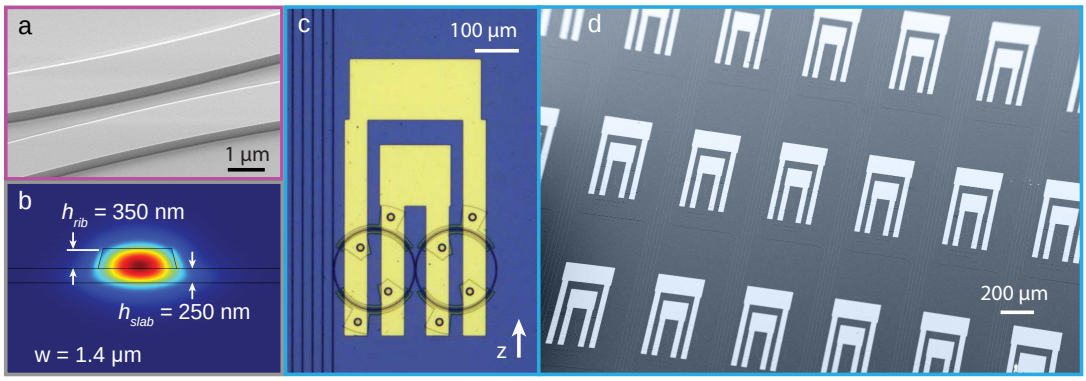

FIG. S-1: **Device details. a**, scanning electron microscope (SEM) image of the gap between the coupled microring resonators. **b**, Cross-section of the optical mode profile in the ring resonator. **c** microscope image of the full device showing the double-ring and microwave electrodes. **d**, SEM image of the array of double ring devices fabricated on a single chip.

The ring resonators of the photonic molecule have waveguide width of 1.4 μm and vary coupling gaps of $\sim$ 700 nm. The coupling waveguides are 800 nm wide by 600 nm thick with a rib height of 350 nm and slab height of 250 nm. This ratio is chosen to ensure optimum electro-optic overlap while still maintaining a tight bending radius.

The high frequency microwave electrodes are designed to achieve differential driving of the two resonators. As shown in figure S-1, the top contact pad is connected to the bottom electrodes of the left ring and the top electrodes of the right ring (and vice versa for the bottom contact pad). Since the LN thin film is x-cut (extraordinary axis z in plane), such configuration allows the electrical field to be in the same direction on each ring, while opposite for the two rings. The electro-optic tuning efficiency is 0.5 GHz/V about half of the value we reported previously as we increased the metal gap to allow minimum perturbation to the high Q optical modes [1]. We pattern 60 programmable photonic molecules on a 10 mm by 8 mm thin film lithium niobate (LN) chip.

The optical properties of the devices are characterized using a tunable telecom laser (Santec TSL-550). The polarization of the light is tuned to TE (in-plane of the chip) before sending into the chip with a lensed fiber. The DC transmission is measured on a 125 MHz photodetector (New Focus 1811A) and the fast oscillation signal is measured on a 12 GHz photodetector (New Focus 1544A) and a fast real-time oscilloscope (Tektronix MSO71604C). Figure S-3 shows the normalized transmission spectrum of the photonic molecule, showing pairs of two-level resonances separated by the free-spectral-range of the microring resonator ($\sim$ 2.2 nm).

The microwave signals are prepared using an arbitrary waveform generator (Tektronix 70001A), which provides synchronized signals to drive the photonic molecule as well as an external modulator and the oscilloscope. The microwave driving signal for the photonic molecule is amplified and sent through an isolator to minimize reflection to the amplifier. A bias-T is used to coupled DC field into the resonator for fine tuning.

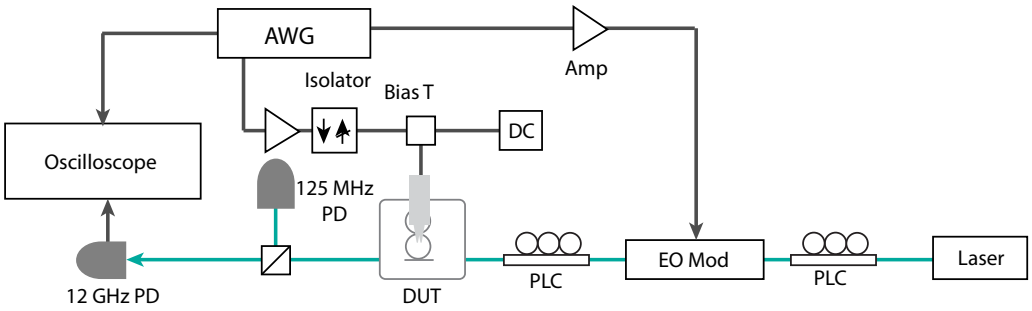

FIG. S-2: **Experimental Setup.** The device is optically pumped by a tunable telecom laser centered around 1630 nm. The light is sent through an external electro-optic modulator and polarization controllers before coupling into the chip with a lensed fiber. The output optical signal, also coupled with a lensed fiber, is sent to a 12 GHz photodetector (New focus 1811A). The converted electrical signal is directed to an oscilloscope. The microwave control signals are generated by an arbitrary wave generator (AWG, Tektronix 70001A) and amplified before sent on to the device. A bias T is used to allow DC control on the microresonators. An electrical isolator is used to capture the electrical reflection from the microresonators. The oscilloscope, device drive signals and modulator drive signals are all synchronized.

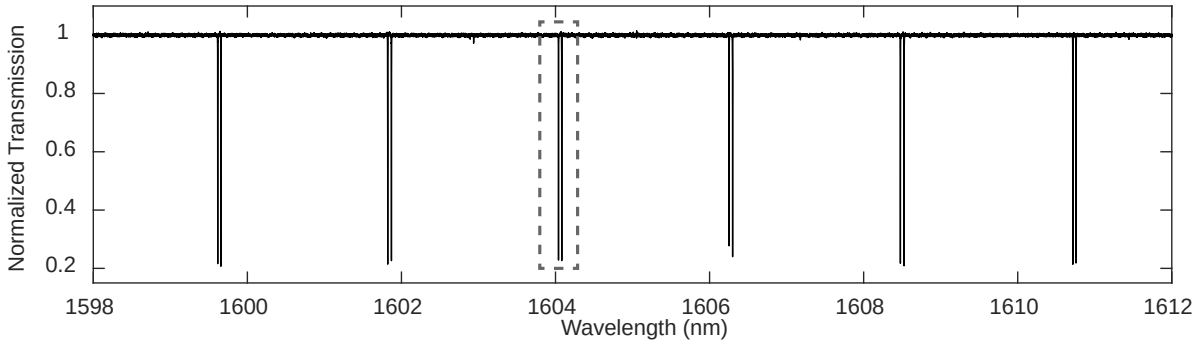

FIG. S-3: **Measured transmission spectrum.** Typical normalized transmission spectra of a double-ring resonator showing pairs of photonic two-level doublets, separated by ~ 2.2 nm of free-spectral-range.

APPENDIX S-2: DESCRIPTION OF THE PHOTONIC MOLECULE

A. System Hamiltonian

The nanophotonic two-level system under a coherent microwave drive can be described by a Hamiltonian with the form

$$\hat{H} = \omega_1 a_1^\dagger a_1 + \omega_2 a_2^\dagger a_2 + \mu(a_1^\dagger a_2 + a_1 a_2^\dagger) + \Omega(a_1^\dagger a_1 - a_2 a_2^\dagger)\cos(\omega_m t) \tag{S-1}$$

where a_1 ($a_1^\dagger$) and a_2 ($a_1^\dagger$) are the annihilation (creation) operators of the two optical modes of the respective microresonator, μ is the coupling strength between the two optical resonators, $\Omega = gV_0$ is the interaction strength of microwave field to the optical resonator, determined by the coupling strength g and microwave peak amplitude V_0. ω_m is the frequency of the microwave modulation.

B. Identical resonator: two bright modes

When the resonant frequencies of the two resonators are identical, i.e. $\omega_1 = \omega_2 \equiv \omega_0$, equation (S-1) can be expressed as

$$\hat{H} = \omega_+ c_1^\dagger c_1 + \omega_- c_2^\dagger c_2 + \Omega(c_1^\dagger c_2 + c_1 c_2^\dagger)\cos(\omega_m t) \tag{S-2}$$

where $\omega_\pm = \omega_0 \pm \mu$, $c_1^{(\dagger)} = \frac{1}{\sqrt{2}}(a_1^{(\dagger)} + a_2^{(\dagger)})$ and $c_2^{(\dagger)} = \frac{1}{\sqrt{2}}(a_1^{(\dagger)} - a_2^{(\dagger)})$.

To simplify the system, we apply a unitary transformation $U_1 = e^{(i\omega_+ c_1^\dagger c_1 t + \omega_- c_2^\dagger c_2 t)}$ and the rotating wave approximation (RWA), we obtain

$$U_1 \hat{H} U_1^\dagger = \frac{\Omega}{2}(c_1^\dagger c_2 e^{i\delta t} + c_1 c_2^\dagger e^{-i\delta t}) \tag{S-3}$$

where the microwave detuning $\delta = \omega_m - \Delta\omega$ and $\Delta\omega$ is the frequency difference between c_1 and c_2. Eqn S-3 is equivalent to the time independent Hamiltonian

$$\hat{H} = \frac{\delta}{2} c_1^\dagger c_1 - \frac{\delta}{2} c_2^\dagger c_2 + \frac{\Omega}{2}(c_1^\dagger c_2 + c_1 c_2^\dagger) \tag{S-4}$$

We obtain the following equations of motion using input-output theory from S-4,

$$\frac{\mathrm{d}}{\mathrm{d}t}\begin{pmatrix} c_1 \\ c_2 \end{pmatrix} = \begin{pmatrix} -i\frac{\delta}{2} & -i\frac{\Omega}{2} \\ -i\frac{\Omega}{2} & i\frac{\delta}{2} \end{pmatrix}\begin{pmatrix} c_1 \\ c_2 \end{pmatrix} \tag{S-5}$$

These equations can also be obtained from a classical treatment using coupled mode theory [2]. We provide the second quantization description to highlight that our system in principle would also work for microwave control of non-classical optical states such single photons, in contrast to previous classical photonic two-level systems that requires optical amplification [3].

C. Autler-Townes Splitting and AC Stark Shifts

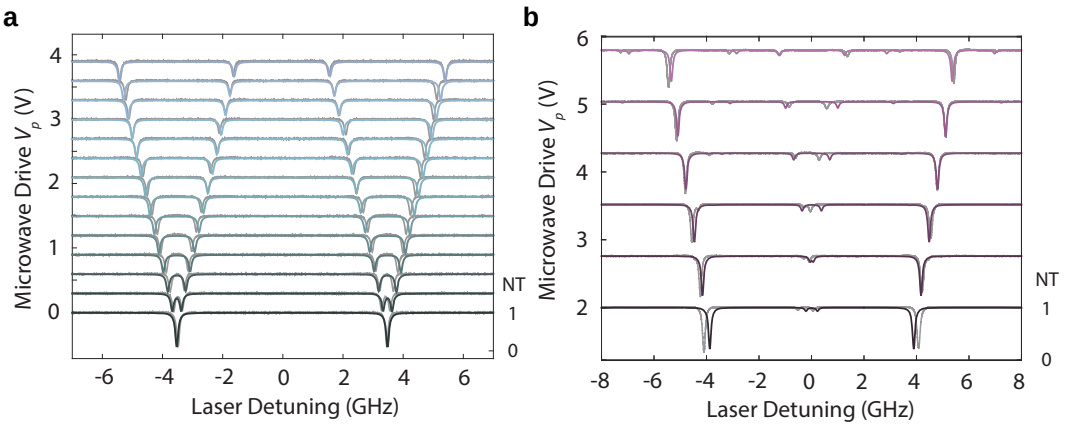

FIG. S-4: **Calculated optical transmission spectrum for Autler-Townes (AT) splitting and AC Stark shift a**, Colored curves: simulated AT spectrum with full mode described in eqn S-2. Gray curves: experimental data as shown in Fig. 2 in the main text. **b**, Colored curves: simulated AC Stark shift spectrum with full mode described in eqn S-2. Gray curves: experimental data.

Under a continuous wave microwave modulation with frequency close to the optical two-mode splitting, each resonance of c_1, c_2 will further split into two dips with splitting frequency

$$W = \sqrt{(\Omega^2 + \delta^2)} \tag{S-6}$$

obtained by diagonalizing the coupling matrix $M = \begin{pmatrix} -i\delta/2 & -i\Omega/2 \\ -i\Omega/2 & i\delta/2 \end{pmatrix}$ from eqn S-5.

For the Autler-Townes splitting measurement data shown in Fig. 2a in the main text and simulation shown in S-4, the microwave modulation signal is on-resonance with the optical two-mode splitting, i.e. $\delta = 0$, with $W = \Omega = gV_0$.

When the microwave frequency detuning to the two-mode resonances is much larger than the driving strength (i.e. $\delta \gg \Omega$), the microwave modulation behaves as a weak perturbation. This perturbation induces a shift of the optical energy levels. Applying the second-order perturbation theory, we have

$$M \approx \begin{pmatrix} -i\left(\frac{\delta}{2}+\frac{\Omega^2}{4\delta}\right) & \\ & -i\left(-\frac{\delta}{2}-\frac{\Omega^2}{4\delta}\right) \end{pmatrix}$$

In the static frame we obtain the shifted frequency:

$$\omega'_{\pm} = \omega_{\pm} \mp \frac{\Omega^2}{4\delta}$$

In the experimental measurements in Fig. 2b and S-4 we have $\delta < 0$ where the two energy levels of c_1, c_2 moves away from each other. For a blue-detuned microwave drive signal, i.e. $\delta > 0$, the two energy levels will move towards to each other.

The calculate optical transmission spectrum for the on-resonance and detuned microwave drive shows good agreement with experimentally measured values (Fig. S-4). The small discrepancies in the peak locations are likely a results from nonlinear response in the laser wavelength scans and bias drift of the double-ring system during the measurements.

D. Optical two-level dynamics

To study the dynamics of the photonic two-level system, we consider the equations of motion S-5 with optical loss and laser input fields. For a single tone optical input on resonance with c_1, the equations of motion are:

$$\dot{c_1} = \left(-i\frac{\delta}{2}-\frac{\gamma}{2}\right)c_1 - i\frac{\Omega}{2}c_2 - \sqrt{\gamma_{\mathrm{ex}}/2}s_{\mathrm{in}} \tag{S-7}$$

$$\dot{c_2} = \left(i\frac{\delta}{2}-\frac{\gamma}{2}\right)c_2 - i\frac{\Omega}{2}c_1 - \sqrt{\gamma_{\mathrm{ex}}/2}s_{\mathrm{in}}e^{\mathrm{i}\omega_m t} \tag{S-8}$$

where γ is the total decay rate of the modes $c_{1,2}$, γ_{ex} is the waveguide coupling rate to mode a_1 and s_{in} is the input laser field. After dropping the fast rotating terms with frequency of ω_m, we obtain the dynamical solution of c_1 and c_2,

$$\begin{aligned} c_1 &= c_{10}e^{-\frac{\gamma}{2}t}\left(\cos\frac{W}{2}t - \mathrm{i}\frac{\delta}{W}\sin\frac{W}{2}t\right) \\ c_2 &= -\mathrm{i}c_{10}e^{-\frac{\gamma}{2}t}\frac{\Omega}{W}\sin\frac{W}{2}t \end{aligned} \tag{S-9}$$

where $c_{10} = \frac{\sqrt{\gamma_{\mathrm{ex}}}s_{\mathrm{in}}}{-i\Delta-\gamma/2}$ is the steady state amplitude in mode c_1 before the microwave is turned on and Δ is the laser detuning. Here $W = \sqrt{\Omega^2+\delta^2}$ is the Autler-Townes splitting frequency as in eqn S-6 and is also the Rabi oscillation frequency. The output power from the waveguide is then

$$\begin{aligned} P_{\mathrm{out}} &= |s + \sqrt{\gamma_{\mathrm{ex}}}a_1|^2 \\ &= |s + \sqrt{\gamma_{\mathrm{ex}}/2}(c_1 + c_2 e^{i\omega_m t})|^2 \end{aligned} \tag{S-10}$$

Substitute eqns S-9 into the expression of the output power and set $\delta = 0$, we obtain

$$P_{\mathrm{out}} = P_{\mathrm{in}}\left|1 - \frac{2\gamma_{ex}}{\gamma}e^{-\frac{\gamma}{2}t}\left(\cos\frac{W}{2}t\right)\right|^2 \tag{S-11}$$

where $P_{\mathrm{in}} = |s|^2$ and we made the approximation to drop the fast rotating terms of c_2 at ~ 7 GHz, as we restrict our measurement bandwidth to ~ 2 GHz. The intra-cavity field can therefore be directly calculated from the output

intensity by $c_1 = (1-\sqrt{P_{\text{out}}/P_{\text{in}}}) \times \gamma/2\gamma_{ex}$. Therefore the real-time AC signal on the photodetector is directly related to the intracavity field c_1. Figure S-5 shows the full numerical solution as of equation S-2, the approximated solution S-11 and the measured photodetector voltage.

We can also estimate the absolute photon conversion efficiency in the optical resonator. Theoretical analysis of the experimentally characterized device shows that $\sim 15\%$ of the optical power is out-coupled after the first pi pulse. $V_\pi = 1.1$ V is assumed, as in the experiment. While the relative frequency conversion efficiency, defined as the ratio of the power in the converted mode (AS) to the power in the pump mode (S) is close to unity, the absolute power output is still limited by the fact that the two modes (S and AS) are undercoupled, as well as their finite cavity lifetime. Using a critically coupled device, and driving at a higher Rabi oscillation frequency, $\sim 90\%$ absolute power outputs from the cavity frequency can be achieved.

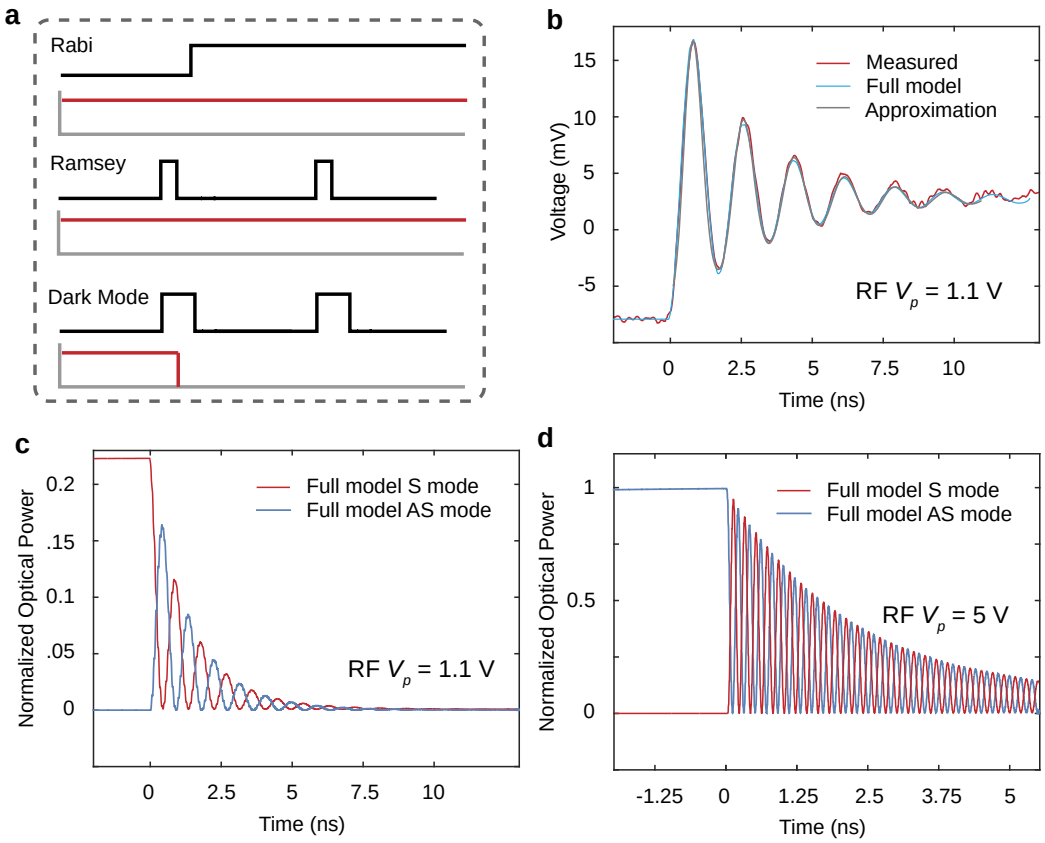

FIG. S-5: **Rabi oscillation, Ramsey interference and dark mode measurements a**, Rabi oscillation is measured in real-time as the microwave signal is turned on. The laser entering the cavity after the turn-on of the microwave signal is negligible as the split optical mode is transparent at the original laser wavelength. Ramsey interference is measured by two time-delayed microwave $\pi/2$ pulses. The optical power is recorded at the end of the second pulse. For the photonic dark mode measurements, the laser is turned off by an external electro-optic modulator for direct detection of optical powers and prevent further coupling into the bright mode during the delay time. **b**, comparison of the measured photodetector voltage, the simulated transmission of the full system and the calculated output from eqn S-11 **c**, Simulated optical power in output waveguides normalized to input optical power for the experimentally measured device. While the frequency conversion efficiency is close to unity, i.e. contrast between the maximum and minimum of the blue and red oscillation curves, the absolute efficiency is $\sim 15\%$, due to the S and AS modes are under-coupled. The optical power is normalized to the input pump power **d**, Critically-coupled S and AS modes can achieve much higher conversion efficiency.

The Ramsey interference is achieved by applying two microwave $\pi/2$ pulses separated by a time delay τ. Here the microwave signal is detuned from the level-splitting by δ. Using the protocol of Ramsey interference and eqn S-7, S-8 , we can get the solution after two $\pi/2$ pulse as a function of time delay τ:

$$c_1(2T+\tau) = e^{-\frac{\gamma}{2}(2T+\tau)} e^{-\mathrm{i}\frac{\delta}{2}\tau} \left[\frac{\Omega^2}{2W^2}(1-e^{\mathrm{i}\delta\tau}) - \mathrm{i}\frac{\delta}{W}\right] c_{10} + e^{-\frac{\gamma}{2}T} e^{-\mathrm{i}\frac{\delta}{2}\tau} \left[1-e^{-\frac{\gamma}{2}\tau}\right] \left[\frac{1}{\sqrt{2}} - \mathrm{i}\frac{\delta}{W}\frac{1}{\sqrt{2}}\right] c_{10} \qquad \text{(S-12)}$$

$$c_2(2T+\tau) = e^{-\frac{\gamma}{2}(2T+\tau)}e^{-\mathrm{i}\frac{\delta}{2}\tau}\left[\frac{\delta\Omega}{2W^2}(e^{\mathrm{i}\delta\tau}-1) - \mathrm{i}\frac{\Omega}{2W}(e^{\mathrm{i}\delta\tau}+2)\right]c_{10} + e^{-\frac{\gamma}{2}T}e^{-\mathrm{i}\frac{\delta}{2}\tau}\left[1-e^{-\frac{\gamma}{2}\tau}\right](-\mathrm{i}\frac{\Omega}{W}c_{10}) \quad \text{(S-13)}$$

where from mode c_1. T is the duration of the $\pi/2$ pulse. The first terms in eqns S-12 and S-13 represent the intra-cavity fields exist in the cavity prior to the arrival of the first $\pi/2$ pulse. The second terms are the leakage of the pump signal into the cavity during the delay, which contributes to a DC term. So the oscillation of the output signal $P_{\text{out}} = \left|s + \sqrt{\gamma_{ex}/2}(c_1 + c_2 e^{i\omega_m t})\right|^2$ rotating at with the frequency δ corresponds to the population of c_1 after dropping the fast rotating terms related to c_2.

E. Optical dark modes

In the case where a_1 and a_2 are far detuned by $\delta\omega \gg \mu$, as in the photon storage and retrieval measurements, we prefer to eliminate the coupling term $\mu(a_1^\dagger a_2 + a_1 a_2^\dagger)$ by a Bogoliubov transformation. Assuming a new basis of c_1, c_2 satisfying:

$$c_1 = va_2 - ua_1$$

$$c_2 = ua_2 + va_1$$

Since c_1, c_2 needs to satisfy the bosonic commutation relationship, we have the condition $u^2 + v^2 = 1$. So we set $u = \cos\frac{\theta}{2}, v = \sin\frac{\theta}{2}$ with $\tan\theta = \mu/\delta\omega$. Then result of this transformation gives us a Hamiltonian for c_1, c_2:

$$\begin{aligned}\hat{H} =& \omega_1 c_1^\dagger c_1 + \omega_2 c_2^\dagger c_2 + \Omega\cos(\omega_m t)\sin\theta(c_1 c_2^\dagger + c_1^\dagger c_2) \\ &+ \Omega\cos(\omega_m t)\cos\theta(c_2^\dagger c_2 - c_1^\dagger c_1)\end{aligned}$$

where $\omega_1 = \omega_0 - \sqrt{\mu^2 + \delta\omega^2}, \omega_2 = \omega_0 + \sqrt{\mu^2 + \delta\omega^2}$. This Hamiltonian indicate that for c_1, c_2, the microwave modulation has a component that induces an exchange interaction $c_1 c_2^\dagger + c_1^\dagger c_2$ and a component that induces a frequency modulation $c_2^\dagger c_2 - c_1^\dagger c_1$.

As for the bright mode pair case we discussed above, i.e. for a small bias $\mu \gg \delta\omega$, a_1, a_2 are nearly degenerate and in c_1, c_2 basis,

$$c_1 \approx -\frac{1}{\sqrt{2}}(a_1 + a_2)$$

$$c_2 \approx \frac{1}{\sqrt{2}}(a_2 - a_1)$$

whereas in the case of a birght-dark optical mode pair, i.e. the bias voltage is high $\mu \ll \delta\omega$, a_1, a_2 have a large frequency difference and in c_1, c_2 basis, c_1 is composed by a large part of a_1 with small part of a_2 and c_2 has large part of a_2 while has only small part of a_1. That means:

$$c_1 \approx -\left(a_1 + \frac{|\mu|}{2\delta\omega}a_2\right)$$

$$c_2 \approx \left(a_2 - \frac{|\mu|}{2\delta\omega}a_1\right)$$

Here the conversion term is finite and is suppressed by a factor $\sin\theta = \frac{\mu}{\delta\omega}$ and the term $\Omega\cos(\omega_m t)\cos\theta(c_2^\dagger c_2 - c_1^\dagger c_1)$ is large, meaning that c_1, c_2 are being frequency modulated. However, Since the modulation frequency is orders of magnitudes larger than the bandwidth of the optical modes, we can neglect this term under high-Q approximation. The resulting Hamiltonian still has a similar form to the bright mode pairs, with a pre-factor $\sin\theta$ in conversion efficiency.

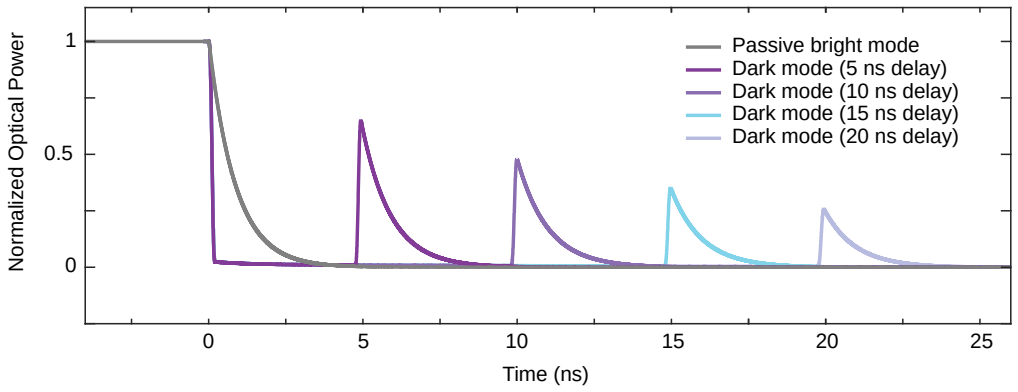

FIG. S-6: **Light storage and retrieval for low-Q bright and high-Q dark mode** The ring is excited and initialized by a CW laser. The pump is switched off at $t = 0$ ns. The gray curve shows the decay of the light if it is stored in the bright mode with a load $Q_{\rm b} = 2 \times 10^6$. The colored curve corresponds to the light retrieved by two π pulse with various delays sequences for a dark mode of $Q_{\rm d} = 2 \times 10^7$.

$$\hat{H}_{\rm dark} = \omega_1 c_1^\dagger c_1 + \omega_2 c_2^\dagger c_2 + \Omega \cos(\omega_m t) \sin\theta (c_1 c_2^\dagger + c_1^\dagger c_2)$$

Similar to the previous section, applying RWA and input-output theory to eqn S-2 E, we obtain

$$\dot{c}_1 = (-\mathrm{i}\omega_1 - \frac{\gamma_1}{2}) c_1 - \mathrm{i}\frac{\Omega}{2} \sin\theta c_2 - \sqrt{\gamma_{\rm ex1}} s_{\rm in} e^{-\mathrm{i}\omega_L t}$$

$$\dot{c}_2 = (-\mathrm{i}\omega_2 - \frac{\gamma_2}{2}) c_2 - \mathrm{i}\frac{\Omega}{2} \sin\theta c_1 - \sqrt{\gamma_{\rm ex2}} s_{\rm in} e^{-\mathrm{i}\omega_L t}$$

where $\gamma_{1,2} = \gamma_i + \gamma_{\rm ex1,2}, \gamma_{\rm ex1} = \gamma_{\rm ex} \cos^2\frac{\theta}{2}, \gamma_{\rm ex2} = \gamma_{\rm ex} \sin^2\frac{\theta}{2}$, γ_i is the internal loss of each ring and $\gamma_{\rm ex}$ is the external loss of ring 1 to waveguide, and $\gamma_{ex1}, \gamma_{ex2}$ are the external losses of modes c_1, c_2 to waveguide. From these equations of motion, we see that at large bias voltages, $\gamma_{ex2} \to 0$ and the access of mode c_2 to the external waveguide is effectively controlled by the microwave drive Ω. At the same time, the life time for mode c_2 becomes closer to that of the intrinsic cavity life time. Therefore, π-pulse control sequences can be implemented as described in the main text to achieve the on-demand photon-storage and retrieval.

The bright mode can be engineered to have a lower Q-factor while the dark mode is detuned far from the bright optical mode. As an example, for an optimized lithium niboate integrated ring resonator with a quality factor similar to previous reported values ($Q \sim 10^7$) [4, 5], set $\delta\omega = 30$ GHz, $\mu = 7$ GHz so $\theta = 0.23$, one could achieve a tunable delay of ~ 15 ns that is more than an order of magnitude better than storing the light in the bright mode (Fig. S-6). For a lithium niboate microresonator that is fabricated close to its material loss limit ($Q \sim 10^9$), one could achieve a tunable storage time of more than 800 ns.

[1] C. Wang, M. Zhang, B. Stern, M. Lipson, and M. Lonar, Optics Express **26**, 1547 (2018).
[2] H. A. Haus and W. Huang, Proceedings of the IEEE **79**, 1505 (1991).
[3] R. J. C. Spreeuw, N. J. van Druten, M. W. Beijersbergen, E. R. Eliel, and J. P. Woerdman, Physical Review Letters **65**, 2642 (1990).
[4] M. Zhang, C. Wang, R. Cheng, A. Shams-Ansari, and M. Lonar, Optica **4**, 1536 (2017).
[5] R. Wu, J. Zhang, N. Yao, W. Fang, L. Qiao, Z. Chai, J. Lin, and Y. Cheng, Optics Letters **43**, 4116 (2018).

Methods

Devices are fabricated on a single-crystalline thin-film lithium niobate layer bonded to a silicon handle wafer with a 2-μm-thick thermally grown silicon dioxide layer on top. Standard electron-beam (e-beam) lithography is used to realize optical waveguide and microresonator patterns in hydrogen silsequioxane e-beam resist. The patterns are then transferred into the lithium niobate layer using argon plasma etching in a standard inductively coupled plasma reactive ion etching tool. The etched depth is 350 nm, leaving a 250-nm lithium niobate slab behind. The slab allows efficient electrical field penetration into the waveguide core region. The first layer of the gold interconnects is patterned by e-beam lithography, and the metals are deposited with e-beam evaporation methods and lift-off processes. Next, a 1.6-μm silicon dioxide layer is deposited on top by plasma-enhanced physical vapour deposition. Finally, metal vias and the top metal layer are realized using standard photolithography followed by e-beam evaporation and lift-off processes[39].

The light from a tunable telecom wavelength laser (SANTEC TSL510) is launched into, and collected from, the lithium niobate waveguides by means of a pair of lensed optical fibres. The microwave control signals are generated from an arbitrary waveform generator (TEKTRONIX AWG70001A) before they are sent to electrical amplifiers. Electrical circulator or isolators are used to prevent multiple electrical reflections. For the Rabi oscillation measurements, the electric field amplitude (c_1) in the S mode is measured by interfering the light out-coupled from the double-ring system with the pump light in the optical waveguide. The interference produces a homodyne signal for c_1 that is sent to a 12-GHz photodiode (Newport 1544A), and owing to the optical frequency difference, the rapid interference signal between the pump light and c_2 can be filtered out electrically with a low-pass filter. For the Ramsey measurements, the optical power is sampled after the second $\pi/2$ pulse using the fast photodiode. For the photon storage measurements, the pump light is synchronously turned off with the first π pulse, allowing direct power readout of the retrieved light and preventing pump further leaking into the bright mode. The modulation on the pump signal is achieved by an external electro-optic modulator synchronized with the microwave control signals. The microwave energy consumption (E_R) for a single Rabi flop can be estimated as $E_R = \frac{1}{2}CV^2 \approx 10\,\mathrm{fJ}$ for the condition in Fig. 3c. The power consumption for continuous Rabi excitation (Fig. 2a) is $P_R = E_R\Omega \approx 60\,\mu\mathrm{W}$, where Ω is the Rabi frequency. In the experiment, since the microwave is generated and terminated with standard 50-Ω impedance elements, the total electrical power consumption is 24 mW, where most of the power is dissipated in the load.

Data availability

The data that support the plots within this paper and other findings of this study are available from the corresponding author upon reasonable request.

References

39. Wang, C., Zhang, M., Stern, B., Lipson, M. & Lončar, M. Nanophotonic lithium niobate electro-optic modulators. *Opt. Express* **26**, 1547–1555 (2018).